HHS Public Access

Author manuscript

Nat Cell Biol. Author manuscript; available in PMC 2018 August 05.

Published in final edited form as:

Nat Cell Biol. 2018 March ; 20(3): 320–331. doi:10.1038/s41556-017-0033-8.

The mTOR-S6K Pathway Links Growth Signaling to DNA Damage Response by Targeting RNF168

Xiaoduo Xie[1,#], **Hongli Hu**[1], **Xinyuan Tong**[1], **Long Li**[1], **Xiangyuan Liu**[1], **Min Chen**[1], **Huairui Yuan**[2], **Xia Xie**[3], **Qingrun Li**[4], **Yuxue Zhang**[1], **Huafang Ouyang**[1], **Mengqi Wei**[5,6], **Jing Huang**[5,6], **Pengda Liu**[7,8], **Wenjian Gan**[7], **Yong Liu**[9], **Anyong Xie**[10], **Xiaoling Kuai**[11], **Gung-Wei Chirn**[12], **Hu Zhou**[13], **Rong Zeng**[4], **Ronggui Hu**[3], **Jun Qin**[2], **Fei-Long Meng**[3], **Wenyi Wei**[7], **Hongbin Ji**[1], and **Daming Gao**[1,*]

[1]State Key Laboratory of Cell Biology, CAS Key Laboratory of Systems Biology, CAS Center for Excellence in Molecular Cell Science, Innovation Center for Cell Signaling Network, Shanghai Institute of Biochemistry and Cell Biology, University of Chinese Academy of Sciences, Chinese Academy of Sciences, 320 Yueyang Road, Shanghai 200031, China

[2]The Key Laboratory of Stem Cell Biology, CAS Center for Excellence in Molecular Cell Science, Institute of Health Sciences, Shanghai Institutes for Biological Sciences, Chinese Academy of Sciences/Shanghai Jiao Tong University School of Medicine, University of Chinese Academy of Sciences, Shanghai 200031, China

[3]State Key Laboratory of Molecular Biology, CAS Center for Excellence in Molecular Cell Science, Shanghai Institute of Biochemistry and Cell Biology, University of Chinese Academy of Sciences, Chinese Academy of Sciences, 320 Yueyang Road, Shanghai 200031, China

[4]CAS Key Laboratory of Systems Biology, CAS Center for Excellence in Molecular Cell Science, Shanghai Institute of Biochemistry and Cell Biology, University of Chinese Academy of Sciences, Chinese Academy of Sciences, 320 Yueyang Road, Shanghai 200031, China

[5]National Center for Protein Science Shanghai, Shanghai Institute of Biochemistry and Cell Biology, University of Chinese Academy of Sciences, Chinese Academy of Sciences, 320 Yueyang Road, Shanghai 200031, China

[6]Shanghai Science Research Center, Chinese Academy of Sciences, Shanghai 201204, China

[*]To whom correspondence should be addressed: Daming Gao, Ph.D., Shanghai Institute of Biochemistry and Cell Biology, Chinese Academy of Sciences, Shanghai 200031, China, Phone: 86-21-54921281; Fax: 86-21-54921293, dgao@sibcb.ac.cn.

[8]Current address: Department of Biochemistry and Biophysics, Lineberger Comprehensive Cancer Center, The University of North Carolina at Chapel Hill, Chapel Hill, NC 27599.

[#]These authors contributed equally to this work.

Author Contribution

X. X., H. H., X. T., and L.L. performed most of experiments with assistance from X.L., M.C., Y.Z., H.O., M.W., J.H., P.L., W.G., Y.L., A. X., X. K., and G.C.. H.Y performed villi length assay of mice after IR treatment under supervision of J. Q. Q.L. and H.Z. performed mass spectrometry analysis under supervision of R.Z.. D.G., X.X., H.H.,W.W., H.J., designed the experiments with input from R.H., and F.M. D.G., X.X., and H.H. wrote the manuscript. All authors commented on the manuscript.

Competing Financial Interests.

The authors declare no competing financial interests.

[7]Department of Pathology, Beth Israel Deaconess Medical Center, Harvard Medical School, Boston, MA 02215

[9]Department of Radiation Oncology, Shanghai General Hospital, Shanghai Jiaotong University, Shanghai 201620, China

[10]Sir Run Run Shaw Hospital and Institute of Translational Medicine, Zhejiang University School of Medicine, Hangzhou, Zhejiang 310016, China

[11]Department of Gastroenterology, Nantong University Affiliated Hospital, Nantong, Jiangsu 226001, China

[12]OrigiMed Inc, Shanghai 201112, China

[13]Department of Analytical Chemistry and CAS Key Laboratory of Receptor Research, Shanghai Institute of Materia Medica, University of Chinese Academy of Sciences, Chinese Academy of Sciences, Shanghai 201203, China

Abstract

Growth signals, such as extracellular nutrients and growth factors, have significant impacts on genome integrity, while the direct underlying link remains unclear. Here we show that the mechanistic target of rapamycin (mTOR)-ribosomal S6 kinase (S6K) pathway, a central regulator of growth signaling, phosphorylates RNF168 at Ser60 to inhibit its E3 ligase activity, accelerate its proteolysis, and impair its function in DNA damage response, leading to accumulated unrepaired DNA and genome instability. Moreover, loss of the tumor suppressor *LKB1/STK11* hyper-activates the mTORC1-S6K signaling and decreases RNF168 expression, resulting in defects of DNA damage response. Expression of a phospho-deficient RNF168 (S60A) mutant rescues the DNA damage repair defects and suppresses tumorigenesis caused by *Lkb1* loss. These results reveal an important function of the mTORC1-S6K signaling in DNA damage response and suggest a general mechanism connecting cell growth signaling to genome stability control.

Introduction

As organisms are often exposed to environmental and internal challenges that cause DNA damage, efficient and accurate DNA repair systems are crucial for maintaining genome integrity and organism subsistence[1, 2]. For instance, Non-homologous end joining (NHEJ) and homologous recombination (HR) are the two major mechanisms responsible for timely and efficient repair of DNA double-strand breaks (DSBs)[3], the most harmful type of DNA damage that is pathologically linked to human diseases such as cancer[4, 5]. Briefly, when DSBs occur, the MRE11-RAD50-NBS1 (MRN) complex initiates signaling cascades by recruiting activated ATM kinase to the lesion sites, which rapidly phosphorylates histone H2A.X (γH2A.X). Then MDC1 is recruited to the damage sites via the interaction between its BRCT domain and phosphorylated γH2A.X to act as a scaffold molecule for E3 ligases RNF8 and RNF168 [6, 7] to build and amplify histone ubiquitination signals. Independent accumulation of 53BP1 and the RAP80-BRCA1 complex will further recruit two different sets of functional factors to initiate NHEJ or HR repair process, respectively. As such, DSBs repair is precisely controlled by delicate and complicated signaling cascades.

mTOR belongs to the phosphatidylinositol 3-kinase-related kinases (PIKKs) family and is an essential regulator of cell homeostasis including protein translation, glucose and lipid metabolism, cell survival and autophagy[8]. Upon activation by extracellular growth signals such as growth factors, amino acids (AA), and insulin, mTOR promotes phosphorylation of hundreds of substrates directly or indirectly via activating downstream kinases including S6K, AKT, PKC and SGK by forming two distinct kinase complexes, mTORC1 and mTORC2, respectively[8]. Thus, mTOR is a central player that senses and responds to various extracellular growth signals. Emerging evidences have indicated metabolic alterations play a role in genome stability control[9, 10], which involves mTOR and its negative regulator such as LKB1[11–18]. However, the underlying molecular link is largely unclear.

In the present study, we found that the mTORC1-S6K pathway regulates DDR through phosphorylation of RNF168 at Ser60, which inhibits its E3 ligase activity to ubiquitinate histone. Furthermore, Ser60 phosphorylation increases RNF168 interaction with TRIP12, leading to enhanced RNF168 degradation. Importantly, depletion of the tumor suppressor LKB1, which causes hyper-activation of mTORC1, dramatically decreases RNF168 abundance and subsequently impairs DDR. Notably, expression of the phospho-deficient RNF168-S60A mutant rescued DDR defects caused by LKB1 depletion, and suppressed tumorigenesis in a mouse lung adenocarcinoma model. Therefore, the mTORC1-S6K pathway may contribute to growth signal-mediated genome instability via inhibition of RNF168 function.

Results

The mTORC1-S6K pathway inhibits DDR

We observed that cells were deficient in repairing DSBs induced by etoposide or ion radiation (IR) in the presence of AA, as evidenced by the sustained levels of γH2A.X and extended lengths of tail moments (Fig. 1a and Supplementary Fig. 1a, b). Given that AA has been shown to activate mTORC1 and its downstream substrate S6K[8, 19], we reasoned that the mTORC1-S6K signaling, a central metabolism regulatory pathway[20], may modulate DDR. To further examine this hypothesis, we challenged *S6k1* and *S6k2* double knockout (*S6k*$^{-/-}$) MEF cells with IR to induce DSBs, and determined the kinetics of cell recovery from DNA damage by monitoring γH2A.X/53BP1 foci, and tail moments of neutral comet assays. Interestingly, enhanced ability to repair damaged DNA, as evidenced by less γH2A.X positive foci and shortened tail moments, were observed in *S6k*$^{-/-}$ cells, compared with wild-type (WT) cells after 2 hours post IR treatment (Fig. 1b–d and Supplementary Fig. 1c). Moreover, an increase in HR-mediated DSB repair was also observed in DR-GFP reporter cells[21], evidenced by more GFP positive cells after S6K1 depletion (Fig. 1e). And more *S6k*$^{-/-}$ cells survived after IR treatment when compared to WT cells (Fig. 1f). These data suggest that S6K may negatively regulate DSB repair in cells.

In supporting for a critical role of S6K in suppressing the ubiquitin signaling upon DNA damage, we observed significantly increased FK2 foci staining for ubiquitin signals in *S6k*$^{-/-}$ cells after IR treatment, compared to control cells (Fig. 1g, h and Supplementary Fig. 1d, e), and re-expression of S6K1 in *S6k*$^{-/-}$ MEF cells reduced FK2 foci after IR (Supplementary Fig. 1f–h). To further examine whether the kinase activity of mTORC1

plays a role in regulating ubiquitin signaling, we observed that rapamycin could rescue the significantly reduced ubiquitin foci upon IR challenge in *Lkb1*$^{-/-}$ MEF cells[22] with hyper-activated mTORC1-S6K signaling (Fig. 1i–k). These data suggest that the kinase activity of mTORC1 is essential in regulating the ubiquitin signaling during DSB repair. It has been reported that the type-A histone poly-ubiquitination at the damage sites is critical for subsequent DSB repair[23–25], thus the mTORC1-S6K signaling may modulate the histone poly-ubiquitination step of DDR to suppress DSB repair.

S6K phosphorylates RNF168 at Ser60

Given that the E3 ubiquitin ligase RNF168[23, 24] was identified and characterized as the key enzyme in generating histone poly-ubiquitination at the DNA damage sites, next we examined whether the mTORC1-S6K signaling may directly phosphorylate and regulate RNF168. To this end, using a proteomic approach, we identified Ser60 phosphorylation in the N-terminal RNF168 as the only phosphorylation responding to AA treatment among total 11 phosphorylation sites identified (Fig. 2a and Supplementary Fig. 2a, b). Using an antibody specifically recognizing the Ser60-RNF168 phosphorylation (pS60-RNF168) (Supplementary Fig. 2c), we found that co-expression with S6K1, or AA stimulation dramatically promoted, while inhibition of the mTORC1-S6K signaling by depletion of S6K1 or rapamycin treatment efficiently blocked, the pS60-RNF168 signal of both endogenous and ectopically expressed RNF168-wild-type (WT), but not the RNF168-S60A mutant (SA) (Fig. 2b–g and Supplementary Fig. 2d). Furthermore, we observed that bacterially purified RNF168-WT, but not RNF168-SA, was efficiently phosphorylated by purified S6K1 kinase, supporting a direct role for S6K in phosphorylating RNF168 at Ser60 (Fig. 2h and Supplementary Fig. 2e). More importantly, *in vitro* phosphorylation of RNF168 could be efficiently blocked by the S6K1 inhibitor PF4708671, but not mTOR inhibitor rapamycin (Fig. 2h). Together, these data suggest that S6K, but not mTORC1, directly phosphorylates RNF168 at Ser60 *in vitro*.

Ser60 phosphorylation impairs RNF168 E3 ligase activity and results in DDR defects

Since the Ser60 residue is adjacent to the RING motif of RNF168, which is critical for its E3 ligase activity[23, 24], we next investigated whether Ser60 phosphorylation influences the function of RNF168 in histone ubiquitination and DNA damage response. Strikingly, compared with RNF168-WT, the phospho-mimetic RNF168-S60E (SE) mutant, failed to promote poly-ubiquitination of both endogenous and transfected H2A, similar to the enzymatic-dead RNF168 (C19S) mutant[24] (Fig. 3a and Supplementary Fig. 2f). These data suggest that Ser60 phosphorylation may interfere with the E3 ligase activity of RNF168. Furthermore, we found that the functional deficiency of RNF168-SE in H2A ubiquitination was largely caused by its reduced E3 ligase activity (Fig. 3b and Supplementary Fig. 2g, h), but not deficiency in discharging the E2-ubiquitin complexes (Supplementary Fig. 2i) [24, 26]. Overall these data indicate that phosphorylation of RNF168 at the S60 residue inhibits its E3 ligase activity.

Next we further examined whether RNF168-Ser60 phosphorylation impairs its major function in DDR such as facilitating the recruitment of 53BP1 to the damage sites[25]. To this end, we generated a tet-inducible RNF168 knock-down HCT116 cell line (Supplementary

Fig. 3a) and reconstituted the cells with shRNA-resistant RNF168 constructs encoding RNF168 WT, SE and SA. We observed less 53BP1 foci in RNF168-SE expressing cells, compared with WT or SA expressing cells (Supplementary Fig. 3b, c), suggesting that S6K-mediated Ser60 phosphorylation inhibits RNF168 E3 ligase activity and subsequently impairs its role in DDR. To more rigorously examine the functional impact of RNF168 Ser60 phosphorylation, we generated *S60A* and *S60E* knock-in (KI) mice by CRISPR/Cas9 technique (Supplementary Fig. 3d), and isolated MEF cells to examine their DDR efficiency after IR treatment. Compared to *WT* and *S60A* KI MEF cells, significantly reduced 53BP1 foci and significantly sustained γH2A.X foci were observed in *S60E* KI MEF cells (Fig. 3c, d and Supplementary Fig. 3e). The deficiency of DNA damage repair was also supported by the observation that the average tail moment of *S60E* KI MEF cells was significantly longer than that of *WT* and *S60A* KI MEF cells in the comet assays post IR (Fig. 3e). Furthermore, increased γH2A.X positive cells were observed in the lung tissue of *S60E* KI mice after IR treatment, while both class switch recombination (CSR) of primary B cells and the average intestinal villi length of *S60E* KI mice post IR treatment were significantly lower than those in WT and *S60A* KI mice (Fig. 3f–j and Supplementary Fig. 3f, g). Cumulatively these data support a significantly impaired and delayed DNA damage repair caused by S6K-mediated RNF168 phosphorylation at Ser60.

The mTORC1-S6K pathway destabilizes RNF168

Interestingly, although there were less RNF168 mRNAs in $S6k^{-/-}$ MEF cells, accumulated RNF168 protein was detected in $S6k^{-/-}$ MEF cells than in WT MEF cells (Fig. 4a, b), which is likely independent of cell cycle or proliferation status (Supplementary Fig. 3h–j). Moreover, RNF168 protein half-life was dramatically extended in $S6k^{-/-}$ MEF cells (Fig. 4c), suggesting that S6K may modulate RNF168 stability. Consistently, depletion of the mTORC1-S6K pathway components, such as mTOR, Raptor or S6K, led to dramatically elevated RNF168 levels (Fig. 4d–f). On the other hand, expression of S6K1 in $S6k^{-/-}$ MEF cells drastically decreased RNF168 levels and delayed the decrease of γH2A.X foci post etoposide treatment (Fig. 4g and Supplementary Fig. 3k). Moreover, MG132 treatment or expressing an enzymatic-dead mutation (KR) of S6K1 kinase could not affect RNF168 stability (Fig. 4h), suggesting that S6K modulate RNF168 stability in a S6K kinase activity and 26S proteasome-dependent manner.

Since RNF168 is phosphorylated by S6K at Ser60, we continued to investigate whether S6K governs RNF168 stability in a Ser60 phosphorylation-dependent manner. To this end, we observed that ectopic expression of S6K1 dramatically shortened the half-life of RNF168-WT, but not the phospho-deficient RNF168-SA mutant (Fig. 4i). Next we examined whether physiological cues modulating the mTORC1-S6K pathway regulate RNF168 protein levels. Interestingly, AA deprivation efficiently inhibited S6K, leading to subsequently increased RNF168 protein levels, which could be reversed by re-addition of AA (Fig. 4j). Similarly, serum re-feeding also quickly activated the mTORC1-S6K signaling and decreased RNF168 expression, which was blocked by rapamycin treatment (Supplementary Fig. 3l). Together, these data demonstrate that the mTORC1-S6K signaling regulates RNF168 protein turnover through phosphorylating RNF168 at Ser60. To determine if there is a pathological correlation between mTORC1 activation and RNF168 expression, we examined the level of

RNF168 and pS6-S240/S244 (pS6)[27] signals, an indicator of mTORC1-S6K pathway activity, in tissue microarrays including clinical non–small cell lung adenocarcinoma samples paired with adjacent normal tissues as controls. Interestingly, RNF168 expression was significantly inversely correlated with pS6 signals (p=0.000329), which was frequently observed in tumor tissues (Fig. 4k, l). In addition, we also observed an inverse correlation between RNF168 levels and pS6 signals in 10 out of 11 lung cancer samples (Supplementary Fig. 3m). The results suggest that RNF168 expression may be negatively associated with activated mTORC1 pathway in pathological conditions. Taken together, these data indicated that activated mTORC1-S6K pathway destabilizes RNF168 in a Ser60 phosphorylation-dependent manner.

Ser60 phosphorylation promotes TRIP12-mediated RNF168 degradation

Since the E3 ligase TRIP12 has been reported as the major E3 ligase governing RNF168 stability[28], we further investigated whether the mTORC1-S6K signaling modulate TRIP12-mediated RNF168 destruction. Notably, siRNA-mediated depletion of TRIP12 completely blocked the decrease and poly-ubiquitination of RNF168 triggered by ectopically expressed S6K1 (Fig. 5a, b), supporting an essential role of TRIP12 in RNF168 ubiquitination and destruction. U2OS cells that stably express Flag-RNF168 were utilized to detect the binding of endogenous TRIP12 to Flag-RNF168 after physiological activation of mTORC1-S6K pathway with insulin, in which the interaction of TRIP12 to RNF168 was dramatically increased by insulin treatment but blocked by rapamycin (Fig. 5c). Furthermore, ectopic expression of S6K1 or AA treatment enhanced the TRIP12 binding to RNF168-WT, but not the RNF168-SA mutant (Fig. 5d, e). Moreover, depletion of TRIP12 led to accumulation of RNF168-SE, but not RNF168-SA abundance (Fig. 5f, g), suggesting that the RNF168 with Ser60 phosphorylation may be a more sensitive substrate for TRIP12. Interestingly, TRIP12 seems to bind RNF168 via its N-terminal region (aa1-749) (Fig. 5h, i). Overall, these results suggest that the mTORC1-S6K signaling governs RNF168 stability in a RNF168-Ser60 phosphorylation and TRIP12-dependent manner.

LKB1 governs RNF168 abundance via the mTORC1-S6K pathway

By phosphorylating AMPK and many other substrates, LKB1 is considered as a major tumor suppressor and metabolism regulator that inhibits the mTORC1-S6K pathway[29]. As LKB1 mutation is frequently observed in various cancers and results in aberrant mTORC1 activation[22, 29], we next explored whether LKB1 depletion has any effect on RNF168 expression, activity and DDR. We observed dramatically reduced RNF168 protein levels in *Lkb1*$^{-/-}$ compared to WT MEF cells, which may due to shortened half-life (Supplementary Fig. 4a, b). In addition, RNF168 levels were significantly reduced upon depletion of LKB1 (Fig. 6a and Supplementary Fig. 4c). Notably, depletion of LKB1 led to increased RNF168-Ser60 phosphorylation levels through activating the mTORC1-S6K pathway (Fig. 6b and Supplementary Fig. 4d). Thus, we reason that activation of the mTORC1-S6K pathway is possibly the major cause of reduced RNF168 expression upon LKB1 loss. In keeping with this notion, inhibition of the mTORC1-S6K signaling by depleting S6K1 or Raptor, restored RNF168 expression in LKB1-depleted U2OS cells (Fig. 6c). Therefore, LKB1 largely modulates RNF168 expression through the mTORC1-S6K pathway.

LKB1 has been implicated to play an important role in DNA damage responses[30], and loss of LKB1 causes decreased DNA repair efficiency[11]. Since RNF168 levels are tightly associated with LKB1 status (Fig. 6a and Supplementary Fig. 4a, b), we next examined whether LKB1 loss, a frequent genetic event in cancer, causes any DDR defects due to reduced RNF168 levels. Consistent with a previous study[12], we found that loss of LKB1 dramatically affected DDR and led to genome instability (Supplementary Fig. 4e–h), which could be rescued by re-expression of LKB1-WT but not a kinase-dead LKB1-KM mutant (Supplementary Fig. 4i, j). To further dissect whether the DDR defects observed in LKB1 depleted cells are due to RNF168 malfunction triggered by activation of the mTORC1-S6K pathway, we expressed RNF168-SA and RNF168-SE mutants in *Lkb1*$^{-/-}$ MEF cells. Upon treatment with IR or etoposide, we found that expression of RNF168-SA (but not RNF168-SE) rescued DDR defects caused by *LKB1* loss (Fig. 6d–h and Supplementary Fig. 4k).

To further investigate the pathological association of LKB1 loss with RNF168 expression and DDR, we examined mouse tumor cells isolated from *Kras*^{G12D}/*p53*$^{-/-}$ and *Kras*^{G12D}/*Lkb1*$^{-/-}$ non–small cell lung cancer (NSCLC) mouse models[31–33]. Compared to *Kras*^{G12D}/*p53*$^{-/-}$cells, *Kras*^{G12D}/*Lkb1*$^{-/-}$cells expressed significantly less amounts of RNF168, and were much more sensitive to ion radiation in the colongenic survival assays and comet assays, which was also well correlated with impaired DDR indicated by γH2A.X and 53BP1 foci imaging experiments (Supplementary Fig. 5a–g).

Expression of RNF168-S60A suppresses tumorigenesis initiated by LKB1 loss

As LKB1 deficiency triggered mTORC1 activation has been linked to cancer initiation and progression, inhibition of RNF168 by mTORC1-S6K may play a significant role in leading to genome instability and eventually tumorigenesis in *LKB1* null background. Consistently, expression of RNF168-SA, but not RNF168-SE, significantly increased 53BP1 foci formation and suppressed xenograft tumor growth in *LKB1* null A549 tumor cells without affecting cell proliferative features (Supplementary Fig. 6a–e). To further investigate the potential role of RNF168-S60 phosphorylation in tumorigenesis within the *Lkb1* loss background, we chose a well established spontaneous NSCLC mouse model (*Kras*^{G12D}/*Lkb1*$^{L/L}$)[33], in which tumors are initiated by CRE excision induced Kras-G12D expression and Lkb1 depletion. As indicated (Fig. 7a), by nasal inhalation method the mice were treated with lentivirus expressing both CRE recombinase and RNF168-SA or RNF168-SE mutant simultaneously. We found that co-expression of RNF168-SA, but not RNF168-SE, dramatically suppressed the tumor number and total tumor burden in all 6 mice tested 10 weeks post treatment (Fig. 7b–d and Supplementary Fig. 6f). Notably dramatically weaker γH2A.X staining was detected in RNF168-SA treated lung tissues (both tumor and non-tumor tissues), indicating that RNF168-SA may inhibit tumorigenesis via promoting DDR (Fig. 7e–g). In order to examine whether depletion of RNF168 in the WT-*Lkb1* background would be sufficient to promote tumorigenesis in combination with Kras-G12D, we performed another similar experiment by treating *Kras*^{G12D} mice with lentivirus expressing CRE and a CAS9-sgRNA system targeting RNF168 (Supplementary Fig. 6g). However, depletion of RNF168 did not significantly increase tumor number or tumor burden (Supplementary Fig. 6h–j). Taken together, the results outlined above suggested that inhibition of RNF168 by mTORC1-S6K pathway may be required for *Lkb1*-loss driven

tumorigenesis, although loss of RNF168 itself is not sufficient to initiate tumorigenesis in wild type LKB1/mTORC1-S6K background.

Discussion

mTOR, the central modulator of cellular homeostasis, has been implicated in genome integrity maintenance, and accumulated evidences have suggested that mTOR inhibition by nutrients and caloric restriction contributes to cancer prevention and extended lifespan [9, 10, 17]. Consistently, there are reports suggesting that the mTORC1 pathway interplays with DNA damage response and repair system[16, 18, 34], although detailed molecular mechanisms are largely unknown. In this study, we characterized a dual-module regulation of RNF168 by the mTORC1-S6K pathway. Ser60 phosphorylation not only inhibits RNF168 intrinsic E3 ligase activity, but also promotes its proteolysis by TRIP12. Since RNF168 is responsible for building up poly-ubiquitin chains to facilitate loading of NHEJ and HR repair complexes at the damage sites, inhibition of RNF168 function would prevent timely repair of DSBs, which may accumulate and subsequently trigger severe genomic defects leading to permanent growth arrest or malignant transformation of cells. Thus, our finding established a molecular link between growth signals and genome stability via phosphorylation of RNF168 by mTORC1-S6K. Interestingly, we observed that RNF168 protein levels were dramatically accumulated within 30 minutes after AA deprivation, and decreased even faster (in 10 minutes) after AA re-feeding (Fig. 4j), indicating that the RNF168 levels are very sensitive to the activation of mTORC1-S6K pathway and it may fluctuate with the amount of nutrients in the extracellular environment. Therefore, inhibition of RNF168 by mTORC1-S6K pathway may also contribute to the genome instability and eventually physiological defects of the organism after long-term uptake of excessive nutrients, in addition to increased production of reactive oxygen species (ROS) by active mTORC1 signaling[35–39].

LKB1/STK11 is a tumor suppressor frequently mutated in various cancers including lung cancer and others[40]. mTORC1 signaling is aberrantly activated after loss of *LKB1* through multiple characterized mechanisms[41–43], and is considered the major mechanism of how *LKB1* loss contributes to oncogenesis. In this study, we identified an association between the LKB1 genetic status and RNF168 protein abundance. Notably, depletion of LKB1 sharply reduces RNF168 levels while inhibition of the mTORC1-S6K pathway efficiently restored RNF168 expression (Fig. 6c), suggesting that the regulation of RNF168 by LKB1 is largely through the mTORC1-S6K pathway. In keeping with low RNF168 expression, *Lkb1* null MEF cells and $Kras^{G12D}/Lkb1^{-/-}$ mouse tumor cells were defective in DDR and more sensitive to IR (Fig. 6e–h and Supplementary Fig. 4e–j and 5b–g). Expression of RNF168-SA that is resistant to mTORC1-S6K mediated inhibition drastically restored DDR defects in *Lkb1* null MEF cells (Fig. 6e–h) and suppressed spontaneous tumorigenesis of $Kras^{G12D}/Lkb1^{L/L}$ NSCLC mouse model (Fig. 7a–g), supporting a crucial role of RNF168 inhibition in tumorigenesis initiated by *LKB1* loss. It is noteworthy that as we treated mice with a lentiviral vector expressing RNF168-SA mutant via nasal inhalation method, and the amount of RNF168-SA protein expressed in mouse lung could not be precisely controlled to physiological levels. Better genetic models may be required to fully evaluate the actual tumor suppressing function of RNF168-SA in *Lkb1* null cancers.

Taken together, our study reveals the mTORC1-S6K-RNF168 signaling axis, by which extracellular growth signals or intrinsic *Lkb1* loss interplays with DNA damage response system (Fig. 7h). Our results also indicate that the mTORC1 signaling not only plays an essential role in supporting tumor cell growth and survival, but also participates in the onset stage of cancer by promoting genome instability. In addition to Ser60 phosphorylation-mediated RNF168 inhibition, additional signaling pathways may also modulate RNF168 function or stability. It would be also interesting to dissect whether certain protein phosphatase(s) specifically protects RNF168 from mTORC1-mediated inhibition through dephosphorylating RNF168-Ser60. Certainly, more research efforts are warranted to fully understand the link between extracellular signals and DNA damage repair systems, and how genome integrity is affected in physiological and pathological conditions.

Methods

Methods, including statements of data availability and any associated accession codes and references, are available in the online version of this paper.

Materials and Methods

Antibodies, chemical inhibitors and plasmids

Primary and secondary antibodies used in this study are listed in Supplementary Table 1. OxiSelect™ Comet Assay Kit (3-Well Slides) (STA-350) was purchased from Cell Biolabs, INC. Myc-Ub, His-Ub, HA-S6K1, HA-S6K1 (KR), shS6K1 constructs were described previously[44]. Flag-RNF168 plasmids were constructed by cloning the corresponding cDNAs into pFLAG-CMV vector. GST-RNF168 and mutants were generated by subcloning into pGEX-4T-1 vector. Retroviral HA-S6K1, Flag-RNF168 and mutants were generated by subcloning into pQCXIH retroviral vector. 6×His-H2A was constructed by cloning H2A.g cDNAs into pET-28a(+) vector. Various RNF168 point mutations (C19S, S60A and S60E) were generated using the QuikChange Site-Directed Mutagenesis Kit (Stratagene) according to the manufacturer's instructions. Lentiviral shRNF168 constructs were generated by inserting shRNF168-1 and shRNF168-2 (sequences were listed in Supplemental Table 2) into pLKO.1 vector. To generate shRNF168-2 resistant FLAG-RNF168 constructs, the underlined silent mutations (AA<u>A</u> CA<u>A</u> TC<u>G</u> GT<u>C</u> AA<u>C</u> AG<u>G</u> AG<u>G</u> AA<u>A</u>) were introduced into the RNF168 coding sequence. Doxycycline-inducible shRNA targeting RNF168 (Tet-On shRNF168) were constructed by subcloning shRNF168-2 target sequence into a modified pLKO.1 vector with doxycycline controlling promoter. All constructs were confirmed by sequencing. shRNA constructs targeting mTOR were from addgene.

Cell culture and generation of DSBs

U2OS, HCT116, A549, HEK293T (293T), Mouse embryo fibroblast (MEF) cells were cultured in DMEM or RPMI 1640 medium with 10% FBS, 100 Units of penicillin and 100 μg/ml streptomycin. U2OS, HCT116, A549, 293T cells were originally from ATCC. All cell lines were examined for mycoplasma free prior experiments. pLKO.1 lentiviral shRNA and pQCXIH retroviral virus packaging and subsequent generation of stable cell lines by infection were performed according to the protocol described previously[45]. For cell viability

assays, cells were plated at 1,000 per well in 96-well plates, and incubated with appropriate medium containing DMSO or DNA damaging agents for 72 hours. Assays were performed with CellTiter-Glo Luminescent Cell Viability Assay Kit according to the manufacturer's instructions (Promega). Amino acids free, glucose free DMEM and amino acids mixture, glucose were ordered from Basal Media. Cycloheximide (CHX.) experiments were performed as described previously[46]. IR was delivered using a ^{137}Cs irradiation source with a dose rate of 1 Gy/min.

Immunoblot and immunoprecipitation (IP)

Cells were lysed in EBC buffer (50 mM Tris pH 7.5, 120 mM NaCl, 0.5% NP-40) with 1mM DTT, protease inhibitors (Roche) and phosphatase inhibitors (Calbiochem.), followed by pulse sonication for 10 seconds. To detect ubiquitination in lysates, 5 mM N-ethylmaleimide (NEM) was added to lysis buffer lacking DTT prior to use. The protein concentrations of lysates were measured using Bio-Rad protein assay kit in a spectrophotometer (Thermo Scientific). Same amounts of whole cell lysates were used for immunoblot (IB). For IP, 1.0 mg of cell lysate was pre-cleared with protein A/G plus Sepharose (Santa Cruz) and then incubated with anti-Flag M2 agarose beads for 2 hours. For endogenous RNF168 IP, 2 μg of RNF168 antibody was incubated with 2 mg pre-cleared cell lysates for 2 hours followed by 1 hour incubation of protein A/G plus Sepharose, then the pellet was washed with lysis buffer for 4 times and analyzed by SDS-PAGE with indicated antibodies.

RNA interference, lentiviral shRNA

The siRNAs were synthesized by Biotend Company (Shanghai, China). All siRNA transfections were performed with X-tremeGENE siRNA Transfection Reagent (Roche) or Lipofectamine 2000 (Invitrogen) at 50 nM final concentration according to the manufacturer's protocol. Oligonucleotide sequences were specified in the Supplemental Table 2. pLKO.1 lentiviral knocking-down vectors to deplete S6K1, mTOR, shLKB1 were described previously[46, 47].

Clonogenic survival assays

Survival curves in clonogenic assays were analyzed using a modified method as described before[48]. Briefly, cells were seeded and exposed to irradiation as indicated in 6-well plates, and cultured for 1–2 weeks after irradiation until visible colonies formed. Then colonies were washed with PBS, fixed and stained with 0.1% crystal violet for 20 minutes. After staining, the plates were washed with distilled water and air-dried. Visible colonies were counted and surviving fractions were calculated by comparing the number of colonies formed in the irradiated cells with no IR treatment control cells.

Immunofluorescence (IF) analysis

Cells were grown on glass coverslips for transfection or treatment as indicated, then treated with ^{137}Cs irradiation with indicated dose 24 hours later, and recovered for the times indicated, fixed with 4% paraformaldehyde in PBS for 15 minutes at room temperature and permeabilized with 0.5% Triton X-100 in PBS for 5 minutes. Samples were rinsed three

times in PBS with 5 minutes each wash. Coverslips were then blocked for 60 minutes with 5% BSA and incubated with primary antibodies for 2 hours. After 3×10 minutes PBS wash, the coverslips were incubated with Alexa-488 conjugated goat anti-rabbit secondary antibody or Alexa-594 conjugated goat anti-mouse secondary antibody (Invitrogen) for 1 hour and washed three times with PBS. Nuclei were counterstained with 4,6-diamidino-2-phenylindole (DAPI) for 10 minutes. Coverslips were rinsed 2×3 minutes with PBS and mounted onto slides using prolong gold anti-fade reagent (Invitrogen). Each sample was counted with 100 cells (each cell nucleus with more than 10 foci unless specifically indicated was considered as positive) for three times, and all images were obtained with Leica TCS SP8 fluorescence microscope.

DR-GFP reporter cell assay

Assays were performed as described previously[49, 50]. Briefly, U2OS DR-GFP reporter cells were transfected with pCBASce-I and indicated siRNAs/constructs. After 48 hours, cells were incubated in sodium butyrate (5 mM) for 16 hours to induce chromatin relaxation before flow cytometry analysis (FACS) to examine GFP positive cells.

Mass spectrometry analysis

To identify RNF168 phosphorylation sites, 293T cells stably expressing Flag-RNF168 were cultured in amino acids (AA) free medium for 3 hours in the presence of 15 μM MG132 and re-fed with AA for 30 minutes before harvest. Cells were pulse sonicated in EBC buffer for 30 seconds and cell lysates were collected to perform Flag IP. The pellet was then resolved on SDS-PAGE and stained by Gelcode™ Blue Safe protein staining reagents (Thermo Scientific). The band corresponding to Flag-RNF168 was excised and sent for mass spectrometry analysis.

Recombinant protein purification

Expression of full length or N-terminal (aa1-200) GST-RNF168 proteins in *E.coli* strain Transetta (DE3) were induced by 0.1 mM IPTG for 20 hours at 18°C, GST tagged proteins were purified using glutathione-Sepharose 4B (Pharmacia) according to the manufacturer's protocol. Purified proteins were dialyzed in E3 buffer (50 mM Tris-HCl pH 8.0, 100 mM NaCl) and concentrated using Amicon Ultra-15 Centrifugal Filter Unit (Millipore, UFC901096). Purification of recombinant 6×His-H2A was performed as described[51]. Briefly, 6×His-tagged histone were induced by 0.1 mM IPTG for 3 hours in *E.coli* strain BL21 at 37°C, then bacteria were harvested and suspended in 50 ml buffer containing of 50 mM Tris–HCl pH8.0, 500 mM NaCl, 1 mM PMSF, and 5% Glycerol. Cells were disrupted by sonication, and centrifuged to collect the pellet which contains insoluble 6×His-tagged histone. The pellets were dissolved in 50 ml of denaturing buffer (50 mM Tris–HCl pH8.0, 500 mM NaCl, 5% glycerol, and 6 M urea), and the resulting lysate was centrifuged to collect the supernatant which contains solubilized 6×His-tagged histone, and nickel–nitrilotriacetic acid (Ni–NTA) agarose beads were added to bind the 6×His-tagged histone. After 120 minutes rotation at 4°C, the beads were washed with denaturing buffer and packed into Econocolumns (Bio-Rad). The purified proteins were dialyzed and concentrated using Amicon Ultra-15 Centrifugal Filter Unit (Millipore, UFC901096).

Acid extraction of histone

Cells were trypsinized down and washed once with cold PBS, suspended in hypotonic buffer (10 mM Tris-HCl pH8.0, 100 mM NaCl, 0.5% NP-40, 1.5 mM $MgCl_2$, and 1 mM DTT, protease inhibitors and 10 μM NEM), and rotated for 15 minutes at 4°C. Nuclear pellets were collected and washed with hypotonic buffer, and then extracted by 0.2 M HCl at 4°C for 12 hours. Extracted histone was precipitated by 33% trichloroacetic acid (TCA) on ice and washed with ice cold acetone twice, then histone pellet was centrifuged and air dried, and dissolved in hypotonic buffer.

In vitro kinase assay

In vitro kinase assays were performed as described previously[44]. Briefly, 2 μg recombinant GST-RNF168 N-terminal proteins were incubated with immunoprecipitated S6K1 from transfected 293T cells in the presence of 200 μM ATP and kinase reaction buffer (20 mM Tris-HCl, 50 mM NaCl, 10 mM KCl, 10 mM $MgCl_2$, 2 mM DTT, pH 7.5) at 30°C for 2 hours. Inhibitors PF4708671 (10 mM), rapamycin (5 mM) and DMSO were added as indicated. Reaction were stopped by boiling in laemmli buffer and analyzed by immunoblotting. For radioactive kinase assay, 5 μg recombinant GST fusion proteins were incubated with S6K1 kinase in the presence of [γ-^{32}P] ATP (5 μCi per reaction) at 35°C for 30 minutes. The reaction was stopped by the addition of SDS loading buffer, resolved on SDS-PAGE, and detected by autoradiography.

In vitro ubiquitination assay

In vitro ubiquitination assay was performed as described before with little changes[52]. Briefly, reaction mixture contains 1 μM GST-RNF168 mutant proteins, 2 μM UbcH5c or Ubc13 (Boston Biochem), 0.5 μM E1 (E-305, BostonBiochem), 45 μM ubiquitin (U-100H, BostonBiochem), 10 mM ATP and 1 μM nucleosome (or 2μM 6×His-H2A) in the presence of 50 mM Tris-HCl (pH 7.5), 100 mM NaCl, 10 mM $MgCl_2$, 1μM $ZnCl_2$ and 1 mM TCEP. The reactions were incubated at 32°C for 3 hours and stopped by SDS-PAGE loading buffer, and were examined by immunoblotting with indicated antibodies or by ponceau S staining.

E2 discharge assay

E2 discharge assay was performed as described before[52]. Briefly, 10 μM ubiquitin charged UbcH5c (E2-802, BostonBiochem) was mixed with 1μM RNF168 proteins (BSA and distilled H_2O as control) in 50 mM Tris-HCl (pH 7.5), 100 mM NaCl, 10 mM $MgCl_2$, 1μM $ZnCl_2$, 1 mM TCEP. The reactions were incubated at 37°C for 30 minutes and stopped by non-reduced SDS-PAGE loading buffer, and analyzed by Gel-code blue stain.

Neutral comet assays

Single-cell gel electrophoretic comet assays were performed under neutral conditions following standard procedures[53, 54]. Cells were seeded the day before IR treatment, and recovered in indicated culture condition for 30 minutes or 3 hours after irradiation (50 Gy). After collected and rinsed twice with ice cold PBS, cells (5×10^5 cells/ml) were mixed with OxiSelect™ Comet Agarose (235002, Cell Biolabs, INC.) at a ratio of 1:3 (v/v) and immediately pipetted onto OxiSelect™ 3-Well Comet Slides (STA-352, Cell Biolabs, INC.).

For cell lysis, the slides were immersed in neutral lysis buffer (2.5 M NaCl, 100 mM Na_2EDTA, 10 mM Tris, pH 7.5, 1% sodium lauroyl sarcosine, 1% Triton-X100 and 10% DMSO) overnight at room temperature. Then, the slides were subjected to electrophoresis at 25 V for 30 minutes, and stained with Vista Green DNA Dye (235003, Cell Biolabs, INC.) for 30 minutes before IF microscopy. At least 100 cells tail moments were analyzed the CometScore software.

Tumor samples and tissue microarray (TMA)

Frozen human lung cancer samples for immunoblotting were performed according to Nantong University Guidelines for Human Research and were approved by the Human Research Ethics Committee (HREC) of Nantong University Affiliated Hospital. The tissue microarray was purchased from Shanghai Outdo Biotech co., LTD (HLug-Ade150Sur-01), and approved by the Human Research Ethics Committee (HREC) of Taizhou Hospital of Zhejiang Province, informed consent was obtained from all subjects. Immunohistochemistry staining was performed by standard protocol with antibodies against RNF168 (ABE367, Millipore) and phospho-S6 ribosomal protein (4858, Cell Signaling Technology).

Animal

All animal experiments were performed following the ethical guidelines and protocols approved by the Institutional Animal Care and Use Committee of the Shanghai Institutes for Biological Sciences, Chinese Academy of Sciences. The procedures used followed the recommendation from the Association for Assessment and Accreditation of Laboratory Animal Care (AAALAC).

Mouse colony, mouse treatment, and tumor analyses

Kras^{G12D} and *Lkb1*$^{L/L}$ mice were originally generously provided by Dr. T. Jacks (Koch Institutefor Integrative Cancer Research, Cambridge, MA), and Dr. R. Depinho (MD Anderson Cancer Center, Houston, TX), respectively. RNF168 *S60A/S60E* knock-in mice were generated with CRISPR/Cas9 technique by Beijing Biocytogen Co., Ltd. All mice were housed in specific pathogen-free (SPF) environment in Shanghai Institute of Biochemistry and Cell Biology. *Kras*^{G12D}/*Lkb1*$^{L/L}$ mice (male and female at 8 weeks of age) were numbered and randomly grouped, and treated with lentivirus expressing Cre recombinase and RNF168 S60A/S60E variants at 2×10^6 PFU by nasal inhalation to perform spontaneous tumorigenesis experiment. Mice were sacrificed at 10 weeks post virus inhalation for gross inspection and histopathological examination. *Kras*^{G12D} mice were treated with Lenti-Cre-Cas9-sgRNA (Tomato or RNF168) at 2×10^4 PFU by nasal inhalation to determine if RNF168 depletion alone would cause tumorigenesis in wile type *Lkb1* background. Then mice were sacrificed at 16 weeks post virus inhalation for gross inspection and histopathological examination.

Class switch recombination assays

Class switch recombination assays was performed as described before[55]. Briefly, WT and RNF168 *S60A/S60E* knock-in mice were sacrificed at the age of 5–6 weeks old and EasySep^{TM} Mouse B Cell Isolation Kit (Stem Cell) was used to purify primary B cells from

spleen. B cells (2×10^6) were stimulated with LPS (20 μg/ml, Sigma) plus recombinant mouse IL-4 (25 ng/ml, novoprotein) for indicated time and the population of IgG1 expressing cells was examined by FACS analysis with a anti-IgG1 antibody (1:200, BD Bioscience) and anti-B220 antibody (1:200, eBioscience).

Hematoxylin and eosin staining and immunohistochemistry (IHC)

Mice lung tissues were inflated with 1 ml 4% paraformaldehyde, fixed overnight and dehydrated in ethanol, embedded in paraffin, sectioned (5μm) and stained with hematoxylin and eosin (Sigma). For IHC staining, slides were deparaffinized in xylene and ethanol, and rehydrated in water. Slides were quenched in hydrogen peroxide (3%) to block endogenous peroxidase activity. Antigen retrieval was performed by heating slides in a microwave for 20 minutes in sodium citrate buffer (pH 6.0). The primary antibodies were incubated at 4 °C overnight followed by using the SPlink Detection Kits (Biotin-Streptavidin HRP Detection Systems) according to the manufacturer's instructions. To calculate the percentages of cells positive for γH2A.X in IHC, totally over 100 high power fields were randomly selected for statistical analysis.

Intestinal villi regeneration assay

8-week-old WT and RNF168 *S60A/S60E* knock-in mice (6 mice per group) were treated with 10 Gy whole body irradiation (WBI) and housed in SPF environment in Shanghai Institute of Biochemistry and Cell Biology. Mice were sacrificed 5 days after WBI and small intestines were used for histological analyses. The length of regenerating villi were quantified (20 fields per genotype using ×20 magnification) after HE staining of paraffin sections.

A549 xenograft tumorigenesis assay

2×10^6 A549 cells in 100 μL PBS were injected into the dorsal flank of 6 week-old randomly grouped (6 mice per group) male BALB/c nude mice. Tumor growth was monitored regularly for up to 50 days by measuring tumor diameters with digital calipers. Tumor volume was calculated by the formula: Volume = $(\text{width})^2\times\text{length}/2$.

Statistics and Reproducibility

The statistical significance of experimental data was determined by two-tailed Student's unpaired t test except significance between RNF168 and pS6 levels in clinical samples was by Chi-square test. $P<0.05$ was considered statistically significant. Individual in vitro experiment was performed three times unless otherwise indicated. For experiments with animal models, the experiments were independently repeated 2 times with similar results. n numbers were indicated in the figure legends. Results were expressed as mean±s.e.m (ns, no significance; *$0.01<p<0.05$, **$0.001<p<0.01$ and ***$p<0.001$). No adjustments were made for multiple comparisons. In vitro experiments were not randomized and the investigators were not blinded to group allocation. In vivo experiments were randomized but the investigators were not blinded to group allocation. Animals were excluded from experiments if they died before the end of experiments and were performed with adequate numbers to ensure statistical evaluation. The data from all experiments were normally distributed and

the variance between groups that were statistically compared was similar. No statistical method was used to predetermine sample size. Sample size was chosen on the basis of literature in the field.

Data availability

Source data for statistic results in Fig. 1b–f,h,j,k, 3c–g,i, 6e,f–h, 7c,d,f,g and Supplementary Fig. 1b,d,e,g, 3b,f–i, 4g,h,j,k, 5c–f, 6b,d–f,h,i, have been provided in Supplementary Table-3. All other data supporting the findings are available from the corresponding author upon reasonable request.

Supplementary Material

Refer to Web version on PubMed Central for supplementary material.

Acknowledgments

We thank Drs. Daniel Durocher, Claudia Lucas, and Lorenza Penengo for sharing RNF168 constructs, and Drs. Kun-liang Guan, Dangsheng Li for critical reading of the manuscript. This work was supported by National Key Basic Research Program of China (2015CB964502), the Strategic Priority Research Program of the Chinese Academy of Sciences (XDB19000000), and grants from National Science foundation of China to D.G. (81372602and 81422033) and to X.X(31401214). P.L. is supported by 1K99CA181342 and 5T32HL007893.

References

1. Langie SA, et al. Causes of genome instability: the effect of low dose chemical exposures in modern society. Carcinogenesis. 2015; 36(Suppl 1):S61–88. [PubMed: 26106144]
2. Ciccia A, Elledge SJ. The DNA damage response: making it safe to play with knives. Molecular cell. 2010; 40:179–204. [PubMed: 20965415]
3. Symington LS, Gautier J. Double-strand break end resection and repair pathway choice. Annual review of genetics. 2011; 45:247–271.
4. Khanna KK, Jackson SP. DNA double-strand breaks: signaling, repair and the cancer connection. Nature genetics. 2001; 27:247–254. [PubMed: 11242102]
5. Jackson SP. Sensing and repairing DNA double-strand breaks. Carcinogenesis. 2002; 23:687–696. [PubMed: 12016139]
6. Huen MS, et al. RNF8 transduces the DNA-damage signal via histone ubiquitylation and checkpoint protein assembly. Cell. 2007; 131:901–914. [PubMed: 18001825]
7. Kolas NK, et al. Orchestration of the DNA-damage response by the RNF8 ubiquitin ligase. Science. 2007; 318:1637–1640. [PubMed: 18006705]
8. Laplante M, Sabatini DM. mTOR signaling in growth control and disease. Cell. 2012; 149:274–293. [PubMed: 22500797]
9. Heydari AR, Unnikrishnan A, Lucente LV, Richardson A. Caloric restriction and genomic stability. Nucleic acids research. 2007; 35:7485–7496. [PubMed: 17942423]
10. Szafranski K, Mekhail K. The fine line between lifespan extension and shortening in response to caloric restriction. Nucleus. 2014; 5:56–65. [PubMed: 24637399]
11. Esteve-Puig R, et al. A mouse model uncovers LKB1 as an UVB-induced DNA damage sensor mediating CDKN1A (p21WAF1/CIP1) degradation. PLoS genetics. 2014; 10:e1004721. [PubMed: 25329316]
12. Ui A, et al. Possible involvement of LKB1-AMPK signaling in non-homologous end joining. Oncogene. 2014; 33:1640–1648. [PubMed: 23584481]
13. Gupta R, Liu AY, Glazer PM, Wajapeyee N. LKB1 preserves genome integrity by stimulating BRCA1 expression. Nucleic acids research. 2015; 43:259–271. [PubMed: 25488815]

14. Alexander A, et al. ATM signals to TSC2 in the cytoplasm to regulate mTORC1 in response to ROS. Proceedings of the National Academy of Sciences of the United States of America. 2010; 107:4153–4158. [PubMed: 20160076]
15. Tripathi DN, et al. Reactive nitrogen species regulate autophagy through ATM-AMPK-TSC2-mediated suppression of mTORC1. Proceedings of the National Academy of Sciences of the United States of America. 2013; 110:E2950–2957. [PubMed: 23878245]
16. Shen C, et al. Regulation of FANCD2 by the mTOR pathway contributes to the resistance of cancer cells to DNA double-strand breaks. Cancer research. 2013; 73:3393–3401. [PubMed: 23633493]
17. Johnson SC, Rabinovitch PS, Kaeberlein M. mTOR is a key modulator of ageing and age-related disease. Nature. 2013; 493:338–345. [PubMed: 23325216]
18. Shen C, et al. TOR signaling is a determinant of cell survival in response to DNA damage. Molecular and cellular biology. 2007; 27:7007–7017. [PubMed: 17698581]
19. Kim DH, et al. mTOR interacts with raptor to form a nutrient-sensitive complex that signals to the cell growth machinery. Cell. 2002; 110:163–175. [PubMed: 12150925]
20. Shimobayashi M, Hall MN. Making new contacts: the mTOR network in metabolism and signalling crosstalk. Nature reviews. Molecular cell biology. 2014; 15:155–162. [PubMed: 24556838]
21. Weinstock DM, Nakanishi K, Helgadottir HR, Jasin M. Assaying double-strand break repair pathway choice in mammalian cells using a targeted endonuclease or the RAG recombinase. Methods in enzymology. 2006; 409:524–540. [PubMed: 16793422]
22. Korsse SE, Peppelenbosch MP, van Veelen W. Targeting LKB1 signaling in cancer. Biochimica et biophysica acta. 2013; 1835:194–210. [PubMed: 23287572]
23. Doil C, et al. RNF168 binds and amplifies ubiquitin conjugates on damaged chromosomes to allow accumulation of repair proteins. Cell. 2009; 136:435–446. [PubMed: 19203579]
24. Stewart GS, et al. The RIDDLE syndrome protein mediates a ubiquitin-dependent signaling cascade at sites of DNA damage. Cell. 2009; 136:420–434. [PubMed: 19203578]
25. Al-Hakim A, et al. The ubiquitous role of ubiquitin in the DNA damage response. DNA repair. 2010; 9:1229–1240. [PubMed: 21056014]
26. Mattiroli F, et al. RNF168 ubiquitinates K13–15 on H2A/H2AX to drive DNA damage signaling. Cell. 2012; 150:1182–1195. [PubMed: 22980979]
27. Ferrari S, Bandi HR, Hofsteenge J, Bussian BM, Thomas G. Mitogen-activated 70K S6 kinase. Identification of in vitro 40 S ribosomal S6 phosphorylation sites. The Journal of biological chemistry. 1991; 266:22770–22775. [PubMed: 1939282]
28. Gudjonsson T, et al. TRIP12 and UBR5 suppress spreading of chromatin ubiquitylation at damaged chromosomes. Cell. 2012; 150:697–709. [PubMed: 22884692]
29. Shackelford DB, Shaw RJ. The LKB1-AMPK pathway: metabolism and growth control in tumour suppression. Nature reviews. Cancer. 2009; 9:563–575.
30. Alexander A, Walker CL. The role of LKB1 and AMPK in cellular responses to stress and damage. FEBS letters. 2011; 585:952–957. [PubMed: 21396365]
31. De Raedt T, et al. Exploiting cancer cell vulnerabilities to develop a combination therapy for ras-driven tumors. Cancer cell. 2011; 20:400–413. [PubMed: 21907929]
32. Calles A, et al. Immunohistochemical Loss of LKB1 Is a Biomarker for More Aggressive Biology in KRAS-Mutant Lung Adenocarcinoma. Clinical cancer research : an official journal of the American Association for Cancer Research. 2015; 21:2851–2860. [PubMed: 25737507]
33. Ji H, et al. LKB1 modulates lung cancer differentiation and metastasis. Nature. 2007; 448:807–810. [PubMed: 17676035]
34. Bandhakavi S, et al. Quantitative nuclear proteomics identifies mTOR regulation of DNA damage response. Molecular & cellular proteomics : MCP. 2010; 9:403–414. [PubMed: 19955088]
35. Schieber M, Chandel NS. ROS function in redox signaling and oxidative stress. Current biology : CB. 2014; 24:R453–462. [PubMed: 24845678]
36. Damsky W, et al. mTORC1 activation blocks BrafV600E-induced growth arrest but is insufficient for melanoma formation. Cancer cell. 2015; 27:41–56. [PubMed: 25584893]

37. Cantor JR, Sabatini DM. Cancer cell metabolism: one hallmark, many faces. Cancer discovery. 2012; 2:881–898. [PubMed: 23009760]
38. Martinez-Outschoorn UE, Peiris-Pages M, Pestell RG, Sotgia F, Lisanti MP. Cancer metabolism: a therapeutic perspective. Nature reviews. Clinical oncology. 2017; 14:113.
39. Wellen KE, Thompson CB. Cellular metabolic stress: considering how cells respond to nutrient excess. Molecular cell. 2010; 40:323–332. [PubMed: 20965425]
40. Katajisto P, et al. The LKB1 tumor suppressor kinase in human disease. Biochimica et biophysica acta. 2007; 1775:63–75. [PubMed: 17010524]
41. Inoki K, et al. TSC2 integrates Wnt and energy signals via a coordinated phosphorylation by AMPK and GSK3 to regulate cell growth. Cell. 2006; 126:955–968. [PubMed: 16959574]
42. Gwinn DM, et al. AMPK phosphorylation of raptor mediates a metabolic checkpoint. Molecular cell. 2008; 30:214–226. [PubMed: 18439900]
43. van Veelen W, Korsse SE, van de Laar L, Peppelenbosch MP. The long and winding road to rational treatment of cancer associated with LKB1/AMPK/TSC/mTORC1 signaling. Oncogene. 2011; 30:2289–2303. [PubMed: 21258412]
44. Liu P, et al. Sin1 phosphorylation impairs mTORC2 complex integrity and inhibits downstream Akt signalling to suppress tumorigenesis. Nature cell biology. 2013; 15:1340–1350. [PubMed: 24161930]
45. Boehm JS, Hession MT, Bulmer SE, Hahn WC. Transformation of human and murine fibroblasts without viral oncoproteins. Molecular and cellular biology. 2005; 25:6464–6474. [PubMed: 16024784]
46. Gao D, et al. Phosphorylation by Akt1 promotes cytoplasmic localization of Skp2 and impairs APCCdh1-mediated Skp2 destruction. Nature cell biology. 2009; 11:397–408. [PubMed: 19270695]
47. Gao D, et al. Cdh1 regulates cell cycle through modulating the claspin/Chk1 and the Rb/E2F1 pathways. Molecular biology of the cell. 2009; 20:3305–3316. [PubMed: 19477924]
48. Franken NA, Rodermond HM, Stap J, Haveman J, van Bree C. Clonogenic assay of cells in vitro. Nature protocols. 2006; 1:2315–2319. [PubMed: 17406473]
49. Pierce AJ, Johnson RD, Thompson LH, Jasin M. XRCC3 promotes homology-directed repair of DNA damage in mammalian cells. Genes & development. 1999; 13:2633–2638. [PubMed: 10541549]
50. Weinstock DM, Nakanishi K, Helgadottir HR, Jasin M. Assaying double-strand break repair pathway choice in mammalian cells using a targeted endonuclease or the RAG recombinase. Methods in enzymology. 2006; 409:524–540. [PubMed: 16793422]
51. Tanaka Y, et al. Expression and purification of recombinant human histones. Methods. 2004; 33:3–11. [PubMed: 15039081]
52. Mattiroli F, et al. RNF168 ubiquitinates K13–15 on H2A/H2AX to drive DNA damage signaling. Cell. 2012; 150:1182–1195. [PubMed: 22980979]
53. Olive PL, Banath JP. The comet assay: a method to measure DNA damage in individual cells. Nature protocols. 2006; 1:23–29. [PubMed: 17406208]
54. Liu C, et al. RNF168 forms a functional complex with RAD6 during the DNA damage response. Journal of cell science. 2013; 126:2042–2051. [PubMed: 23525009]
55. Bohgaki T, et al. Genomic instability, defective spermatogenesis, immunodeficiency, and cancer in a mouse model of the RIDDLE syndrome. PLoS genetics. 2011; 7:e1001381. [PubMed: 21552324]

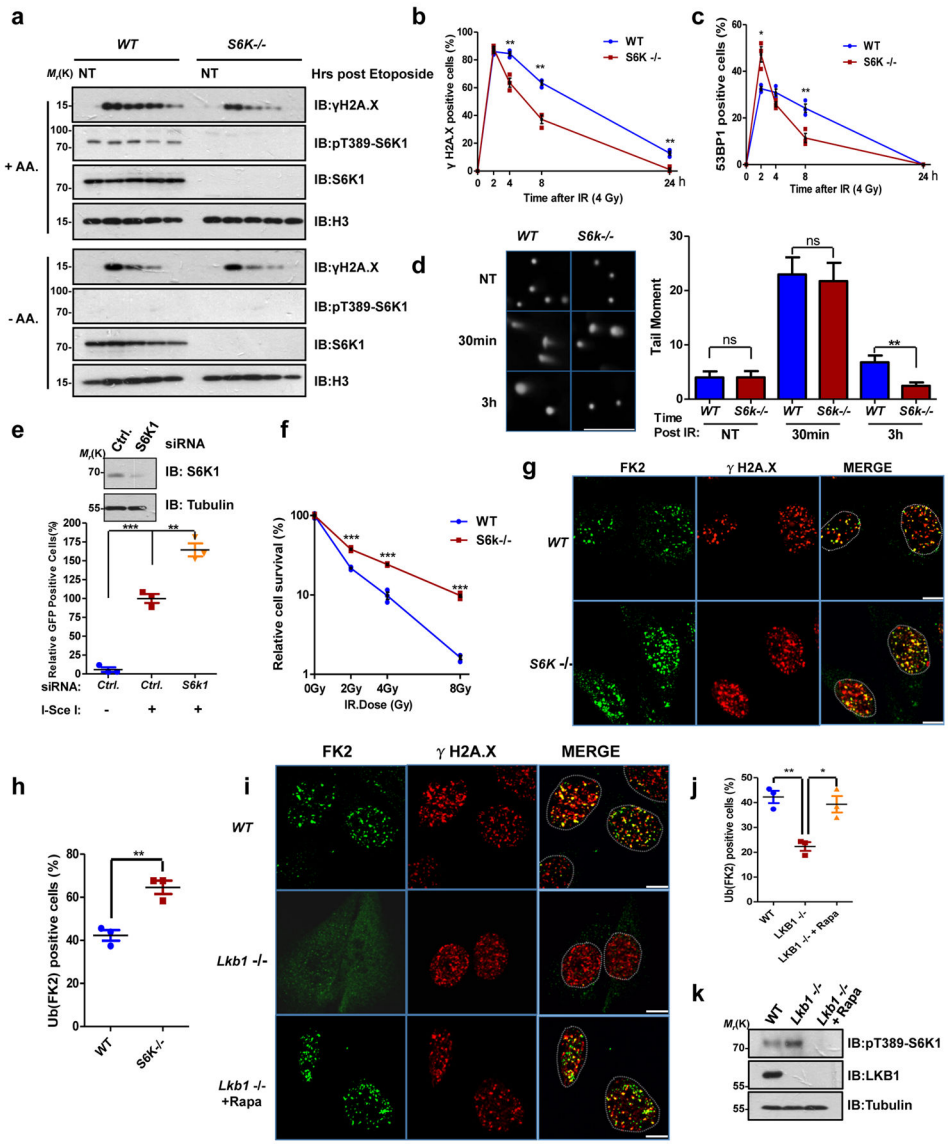

Figure 1. mTORC1-S6K signaling suppresses DNA damage response

(a) Immunoblotting (IB) of cell lysates from wild-type (WT) and *S6k*$^{-/-}$ MEF cells treated with 20 μM etoposide for 2 hours and collected at indicated time after recovery in the presence/absence of amino acids (+/−AA.). **(b–c)** Percentage of WT and *S6k*$^{-/-}$ MEF cells fixed at indicated time after IR (4 Gy) treatment and stained for γH2A.X (**b**) and 53BP1 (**c**) foci. The percentage of positive cells (>10 foci) among 100 cells for each sample were calculated and plotted. Results are from n=3 independent repeats. Related to Supplementary Fig. 1c. **(d)** WT and *S6k*$^{-/-}$ MEF cells were harvested for neutral comet assay at indicated time after IR (50 Gy) treatment. Scale bars, 5 μm. Cell numbers of NT (no treatment): WT, n=105; *S6k*$^{-/-}$, n=98 cells. 30 min post IR: WT, n=154; *S6k*$^{-/-}$, n=131 cells. 3h post IR: WT, n=216; *S6k*$^{-/-}$, n=174 cells. The results were from a single experiment. **(e)** U2OS/DR-GFP reporter cells were transfected with indicated plasmids and the percentage of GFP positive cells were determined by FACS analysis 48 hours post transfection (n=3

independent experiments). **(f)** Relative cell survival of WT and *S6k*$^{-/-}$ MEF cells exposed to indicated doses of IR (n=3 independent experiments). **(g–h)** Representative images (**g**) and quantification (**h**) (n=3 independent experiments) of conjugated ubiquitin (Ub, FK2) foci positive WT MEF cells and *S6k*$^{-/-}$ cells 2 hours after IR (4 Gy) treatment. Scale bars, 10 μm. **(i–k)** Representative images (**i**) and quantification of FK2 (**j**) in WT and *Lkb1*$^{-/-}$ MEF cells. As indicated, *Lkb1*$^{-/-}$ MEF cells were pretreated with/without rapamycin (Rapa., 50 nM) for 1 hour before exposed to IR (4 Gy) treatment. Cells were fixed for immunofluorescence (IF) experiments 2 hours post IR (n=3 independent experiments). Scale bars, 10 μm. Effects of rapamycin treatment was validated with indicated antibodies (**k**). Unpaired student's t test is used (ns, no significance; *0.01<p<0.05, **0.001<p<0.01 and ***p<0.001) and data were shown mean ± s.e.m. Statistics source data can be found in Supplementary Table 3. The immunoblots are representative of three independent experiments. Unprocessed original scans of blots are shown in Supplementary Fig. 8.

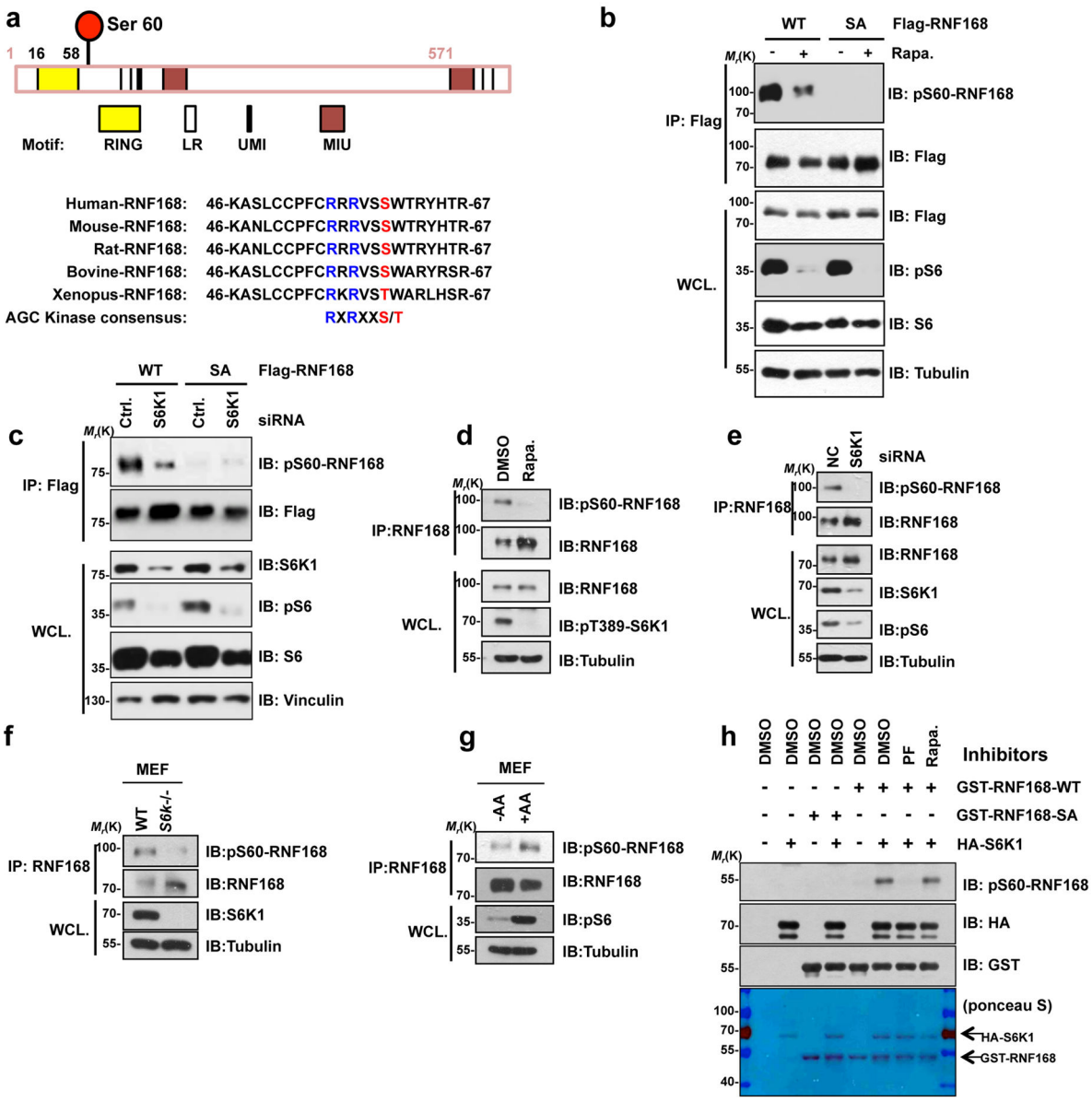

Figure 2. S6K phosphorylates RNF168 at Ser60

(a) A schematic structure of RNF168 and the position of Ser60 phosphorylation site (top). Ser60 site is conserved in many animal species and matches the consensus motif of AGC kinases (bottom). **(b)** IB analysis of whole cell lysates (WCL) and Flag-immunoprecipitation (IP) from 293T cells transfected with Flag-RNF168 WT or SA constructs. 20 nM rapamycin (Rapa.) or DMSO were added 12 hours before cell harvest. **(c)** IB analysis of WCL and Flag-IP with indicated antibodies from 293T cells transfected with indicated Flag-RNF168 constructs and siRNAs. **(d–e)** IB analysis of WCL and endogenous RNF168 IP derived from 293T cells pre-treated with 50 nM rapamycin (**d**) or transfected with S6K1 siRNA (**e**). **(f)** IB analysis of WCL and endogenous RNF168-IP derived from WT and *S6k*$^{-/-}$ MEF cells with indicated antibodies. **(g)** IB analysis of WCL and endogenous RNF168-IP derived from WT MEF cells treated with/without AA with indicated antibodies. **(h)** Recombinant GST-

RNF168 proteins were incubated with purified HA-S6K1 to perform *in vitro* kinase assay in the presence of ATP and kinase inhibitors (PF4708671 (PF), 10 mM or rapamycin (Rapa.), 5 mM) as indicated. The products were stained with ponceau S first and then detected with indicated antibodies. The immunoblots are representative of three independent experiments. Unprocessed original scans of blots are shown in Supplementary Fig. 8.

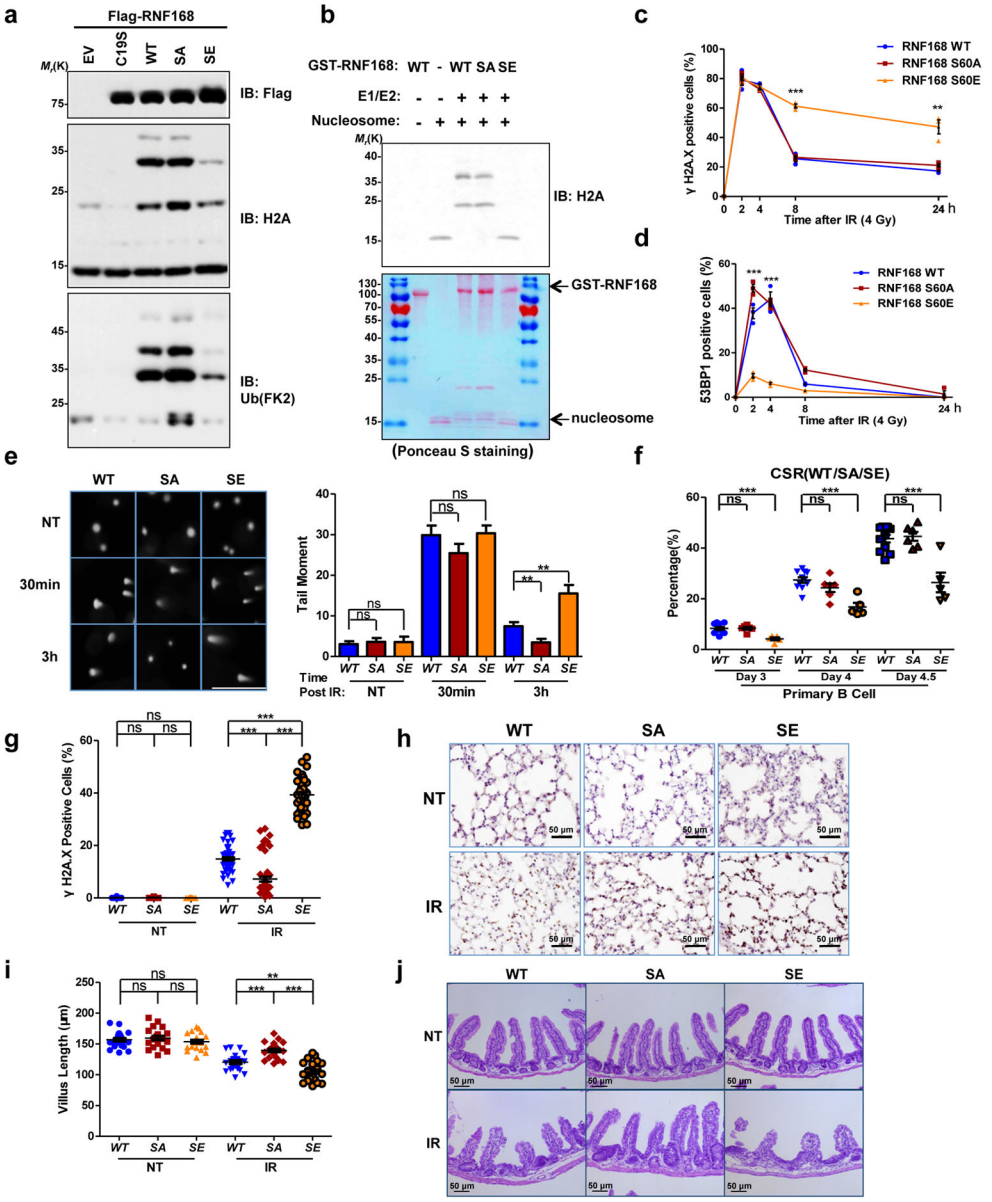

Figure 3. Ser60 phosphorylation inhibits RNF168 function and impairs DNA damage repair

(a) IB analysis of histone extracts from 293T cells transfected with indicated constructs. **(b)** Recombinant GST-RNF168 proteins were incubated with mononucleosome in the presence of E1/E2 for *in vitro* ubiquitination assays. The products were stained with ponceau S first and then detected with indicated antibodies. **(c–d)** Quantification of WT and *S60A/S60E* knock-in MEF cells fixed at indicated time after IR (4 Gy) treatment and stained for γH2A.X (**c**) and 53BP1 (**d**) foci. The percentage of positive cells (>10 foci) among 100 cells for each sample were calculated and plotted. Results are from n=3 independent repeats, related to Supplementary Fig. 3e. **(e)** Neutral comet assays with WT and *S60A/S60E* knock-in MEF cells harvested at indicated time after IR (50 Gy) treatment. Scale bars, 5 μm. Cell numbers analyzed for NT (no treatment): WT, n=114; *SA*, n=130; *SE*, n=148 cells. 30 min post IR: WT, n=148; *SA*, n=157; *SE*, n=189 cells. 3h post IR: WT, n=138; *SA*, n=102; *SE*,

n=181 cells. The results were from a single experiment. **(f)** FACS analysis of primary B cells expressing IgG1 from WT and *S60A/S60E* knock-in mice and stimulated with LPS (20 μg/ml) and IL-4 (25 ng/ml) for indicated days to determine antibody class switch recombination (CSR) efficiency. The number of mice analyzed: WT, n=11; *SA*, n=6; *SE*, n=5 mice. **(g–h)** Statistical analysis (**g**) and representative images (**h**) of γH2A.X immunohistochemistry (IHC) staining in lung sections from WT and *S60A/S60E* knock-in mice (6 mice for each group) 5 days post irradiation treatment (10Gy). Scale bars, 50 μm. Sections numbers analyzed for NT: WT, n=23; SA, n=20; SE, n=15 sections. For IR group: WT, n=53; SA, n=58; SE, n=36 sections. The results were from a single experiment. **(i–j)** Quantification (**i**) and representative images (**j**) of intestinal regenerating villi from mice in **(g–h)**. n=20 fields per genotype were analyzed (×20 magnification) after HE staining. Scale bars, 50 μm. Unpaired student's t test is used (ns, no significance; **0.001<p<0.01 and ***p<0.001) and data were shown mean ± s.e.m. Statistics source data can be found in Supplementary Table 3. The immunoblots are representative of three independent experiments. Unprocessed original scans of blots are in Supplementary Fig. 8.

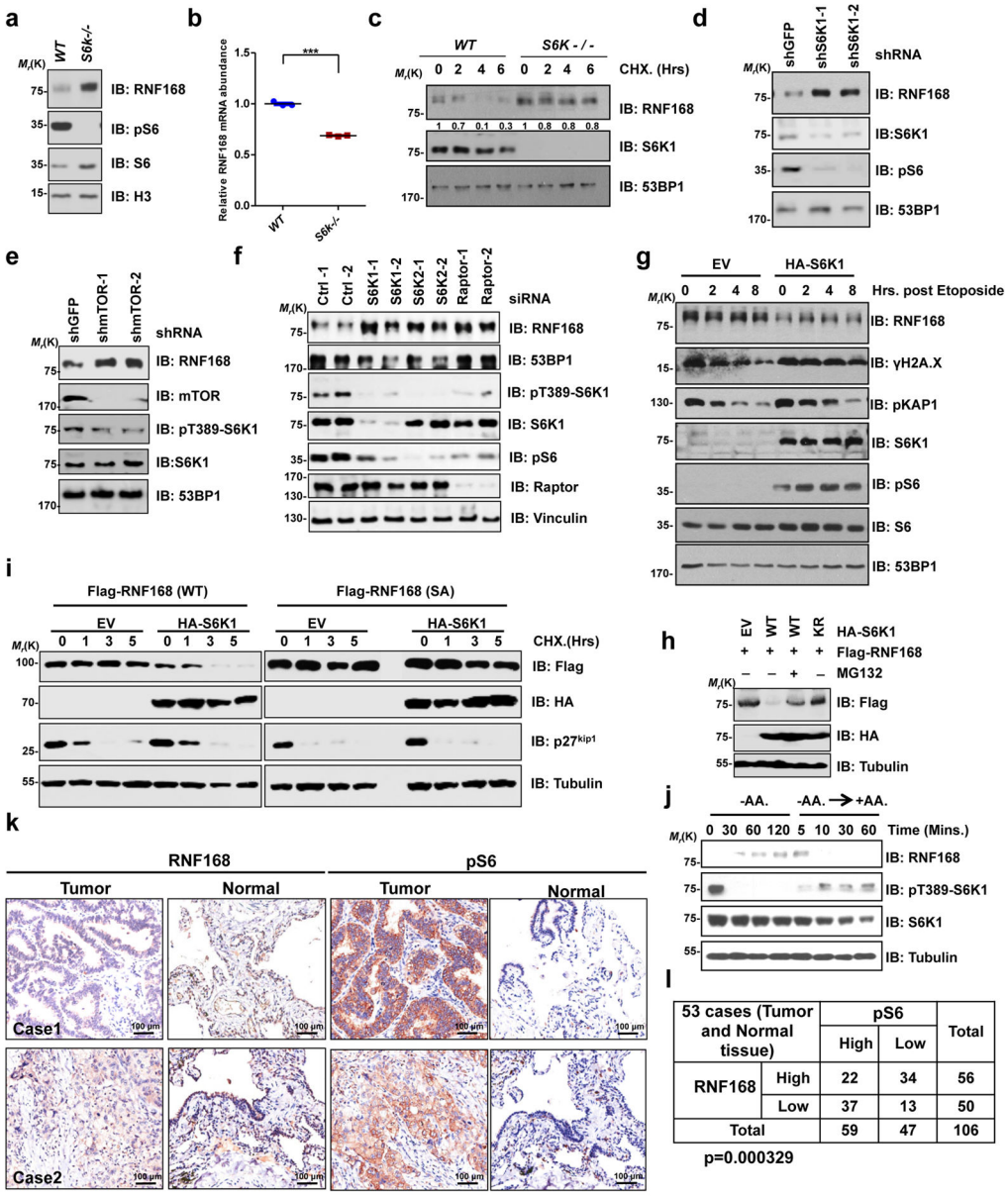

Figure 4. RNF168 Ser60 phosphorylation promotes its degradation

(a–b) Protein and mRNA levels of RNF168 were determined by IB analysis and q-PCR from WT and *S6k*$^{-/-}$ MEF cells. **(c)** Half-life of RNF168 protein in WT and *S6k*$^{-/-}$ MEF cells. CHX, cycloheximide, 100 μg/ml. **(d)** IB analysis of WCL from U2OS cells infected with lenti-viral shS6K1 or shGFP. **(e–f)** IB analysis of WCL from U2OS cells treated with indicated shRNAs (**e**) or with indicated siRNAs **(f). (g)** IB analysis of *S6k*$^{-/-}$ MEF cells infected with virus expressing HA-S6K1 or empty vector (EV). Cells were harvested at indicated time after 20 μM etoposide treatment. **(h)** IB analysis of WCL from 293T cells transfected with indicated constructs. Cells were treated with/without 15 μM MG132 for 12 hours before harvest. KR, A kinase-dead version of S6K1 construct. **(i)** Half-life of Flag-RNF168 in 293T cells transfected with indicated plasmids. 36 hours after transfection, CHX

(100 μg/ml) was added and cells were harvested at indicated time points for IB analysis. **(j)** 293T cells were cultured in amino acids free (-AA.) medium for indicated period of time, then were harvested directly or at indicated time points after re-addition of amino acids (+AA.) for IB analysis. **(k–l)** Representative images of RNF168 and pS6 signals in tissue microarrays containing 53 sets of clinical lung adenocarcinoma tissues and paired adjacent normal tissues as assessed by IHC. Both RNF168 and pS6 levels were classified as low and high based on the intensities of the IHC staining, and the number of tissues classified in each category are depicted in the tabulation in (**l**). Chi-square test was used to support a significant inverse correlation (p=0.000329, 95% CI is from 0.369 to 0.765) between RNF168 and pS6 levels in clinical samples. The numbers of samples with high/low RNF168 and pS6 levels are indicated. Scale bars, 100 μm. Unpaired student's t test is used for (**b**) (***p<0.001) and data were shown mean ± s.e.m. Statistics source data can be found in Supplementary Table 3. The immunoblots are representative of three independent experiments. Unprocessed original scans of blots are in Supplementary Fig. 8.

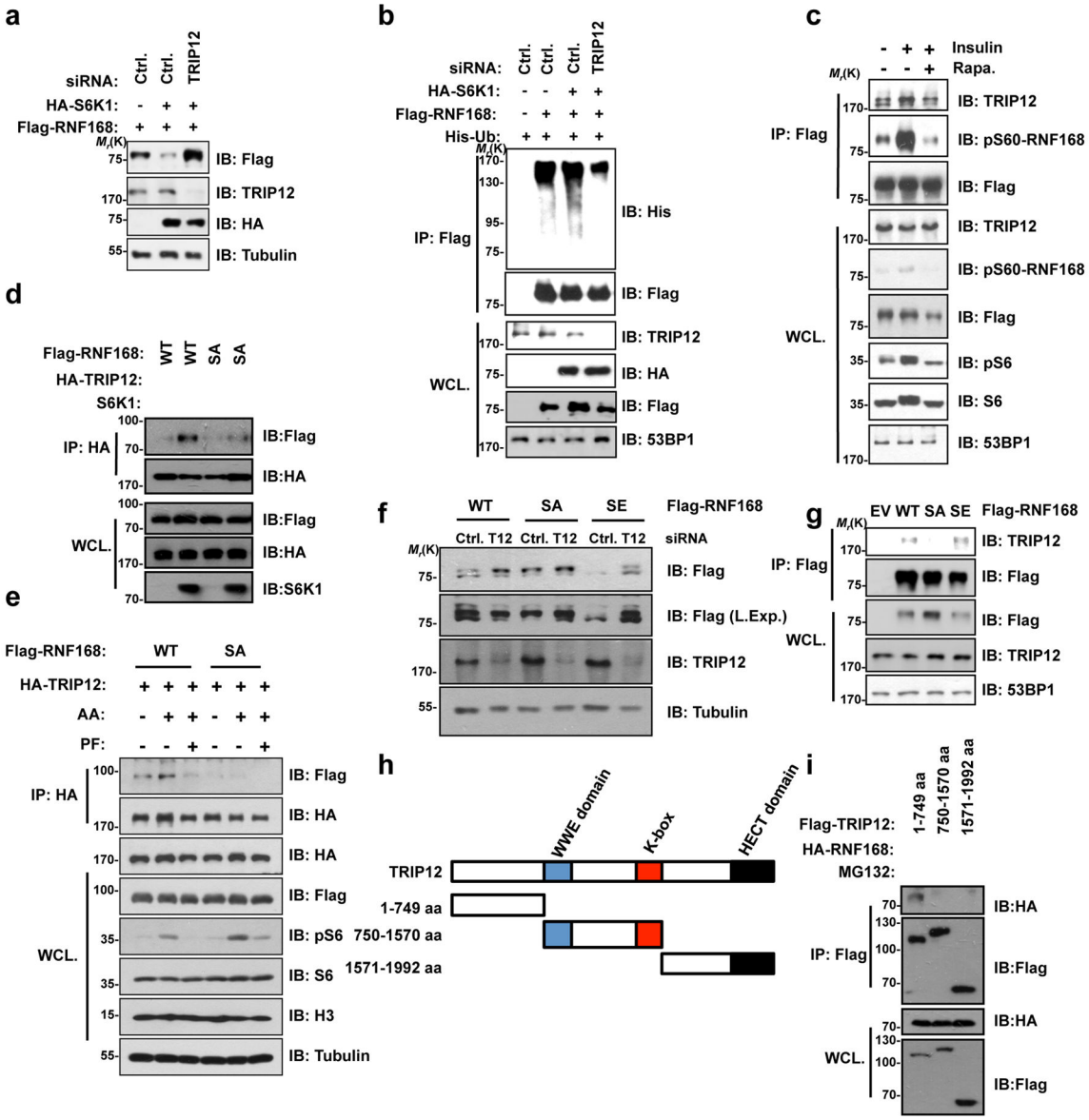

Figure 5. Ser60 Phosphorylation destabilizes RNF168 in a TRIP12-depended manner

(a–b) IB analysis of WCL and Flag-IP from 293T cells co-transfected with indicated siRNAs and constructs. A mixture of two independent siRNAs targeting TRIP12 and control siRNA (Ctrl) were used. 12 hours before harvest for Flag-IP, 15μM MG132 was added to the cells in (**b**). **(c)** U2OS cells expressing Flag-RNF168-WT were serum starved and treated with 15μM MG132 for 12 hours before addition of insulin (45 μg/ml) and rapamycin (Rapa., 50 nM). 30 minutes later, cells were harvested for Flag-IP and IB analysis with indicated antibodies. **(d)** IB analysis of HA-IP and WCL from 293T cells co-transfected with indicated constructs. **(e)** IB analysis of HA-IP and WCL from 293T cells transfected with indicated constructs and treated with AA and PF4708671 (PF, 10μM). 36 hours after transfection, cells were cultured in AA free medium for 3 hours before treated with AA and PF for another 30 minutes. Then cells were harvested for HA-IP and IB analysis as

indicated. **(f)** IB analysis of WCL from 293T cells co-transfected with RNF168 constructs and siRNAs targeting TRIP12 (T12) or control (Ctrl.) as indicated. **(g)** IB analysis of Flag-IP and WCL from U2OS stable cell lines expressing Flag-RNF168 variants with indicated antibodies. 12 hours before harvest, 15μM MG132 was added to the cells. **(h)** A schematic structure of TRIP12 truncation constructs. **(i)** IB analysis of Flag-IP and WCL from 293T cells transfected with HA-RNF168 and Flag-TRIP12 constructs as indicated in (**h**). The immunoblots are representative of three independent experiments. Unprocessed original scans of blots are in Supplementary Fig. 8.

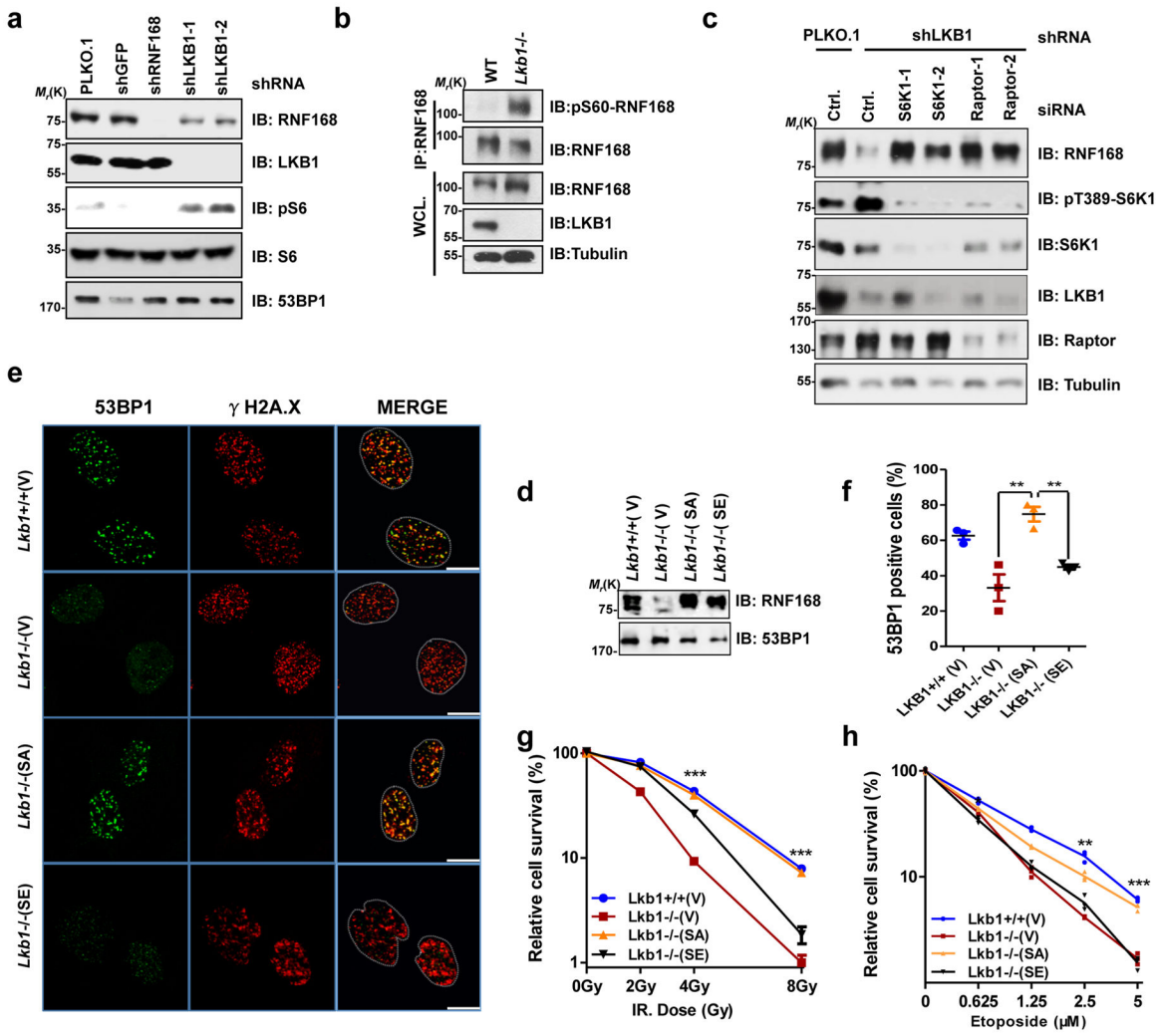

Figure 6. Inhibition of RNF168 by mTORC1-S6K contributes to DDR defects caused by *Lkb1* loss

(a) IB analysis of WCL derived from U2OS cells infected with lenti-viral shRNAs targeting RNF168 or LKB1. **(b)** IB analysis of endogenous RNF168-IP and WCL derived from WT and *Lkb1*$^{-/-}$ MEF cells. **(c)** U2OS cells were first stably infected with PLKO vector or lenti-viral shRNAs targeting LKB1, and then transfected with indicated siRNAs. 48 hours after transfection, WCL were made for IB analysis with indicated antibodies. **(d)** IB analysis of RNF168 in WT and *Lkb1*$^{-/-}$ MEF cells that infected with empty vector (V) or RNF168 S60A (SA)/RNF168 S60E (SE) expressing lenti-virus. **(e–f)** Representative images (**e**) and quantification of 53BP1 foci (**f**) in resulting MEF cells from (**d**). The percentage of positive cells (>10 foci) among 100 cells for each sample were calculated and plotted. Results are from n=3 independent experiments. Scale bars, 10 μm. **(g–h)** Indicated MEF cells from (**d**) were split by the limited dilution and exposed to indicated doses of IR (**g**) or etoposide treatment (**h**). 7 days later, the dishes were stained with crystal violet and visible colonies were counted and plotted. Results are from n=4 independent experiments in **(g)** and from n=3 independent experiments in **(h)**. Panels in (**a**–**d**) are representative of 3 experiments.

Unpaired student's t test is used for (**f–h**) (**0.001<p<0.01 and ***p<0.001) and data were shown mean ± s.e.m. Statistics source data can be found in Supplementary Table 3. Unprocessed original scans of blots are in Supplementary Fig. 8.

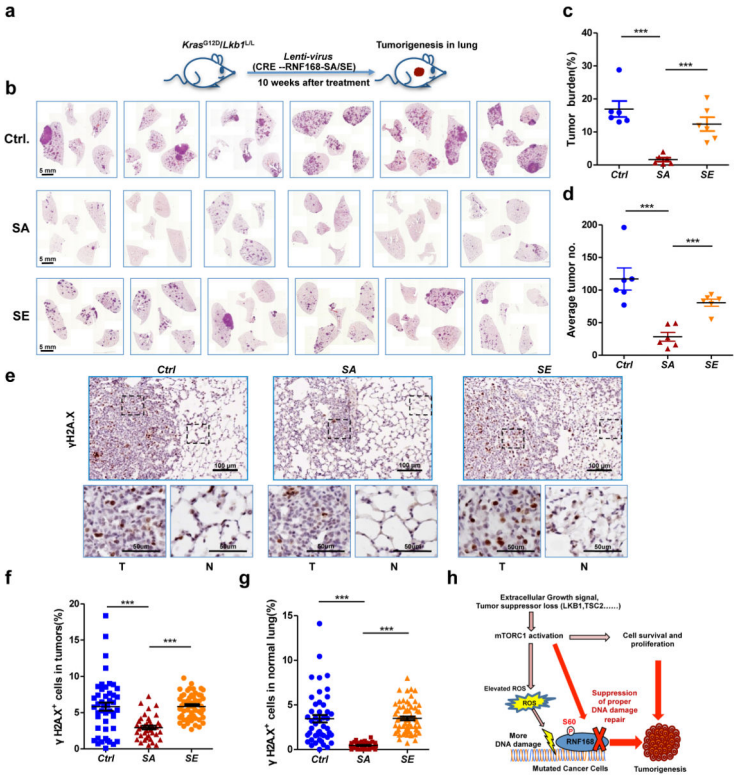

Figure 7. Phospho-deficient RNF168-SA mutant suppresses tumorigenesis in *Kras*^{G12D}/*Lkb1*$^{L/L}$ mice NSCLC model

(a) Schematic model of lung tumorigenesis from *Kras*^{G12D}/*Lkb1*$^{L/L}$ mice treated with lenti-CRE-RNF168 virus. 10 weeks after nasal inhalation, mice were sacrificed and analyzed. **(b)** Tumor histology images from all the mice treated in (**a**). Scale bar, 5 mm (n=6 mice for each group). **(c–d)** The total tumor burden (**c**) and average tumor numbers (**d**) from (**a**) were calculated and plotted (n=6 mice for each group). **(e)** Representative images for γH2A.X IHC staining in lung tissues from (**b**). Scale bar, 100 μm (50 μm in the magnification). T, tumor; N, normal lung tissue next to tumor nodules. **(f–g)** Statistical analysis of γH2A.X IHC staining in *Kras*^{G12D}/*Lkb1*$^{L/L}$ mice lung tumor sections (**f**) and normal lung (**g**) from (**a**). Section numbers for analysis in **(f)**: Ctrl, n=47; SA, n=39; SE, n=52 sections. And for analysis in **(g)**: Ctrl, n=47; SA, n=48; SE, n=65 sections. Data are collected from 6 mice in each group. **(h)** Proposed model for how phosphorylation of RNF168, caused by extracellular growth signals and tumor suppressors loss and subsequent mTORC1 activation, impairs proper DNA damage repair in mutated cancer cells and therefore contributes to tumorigenesis. The experiments in panels **(a–g)** were performed twice. Unpaired student's t test is used for (**c–d**) and (**f–g**) (***p<0.001) and data were shown mean ± s.e.m. Statistics source data can be found in Supplementary Table 3.